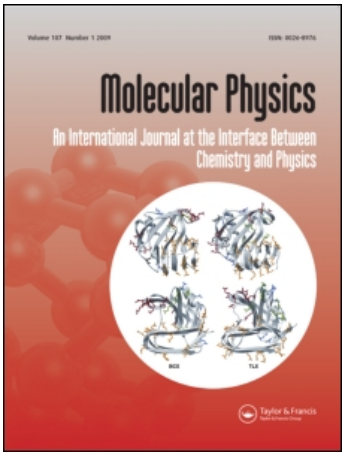

Molecular Physics
Publication details, including instructions for authors and subscription information:
http://www.informaworld.com/smpp/title~content=t713395160

The rotational-vibrational spectrum of symmetric non-rigid triatomics in hyperspherical coordinates: the H^+_3 molecule

P. Bartlett[a]; B. J. Howard[b]
[a] School of Chemistry, Cantocks Close, Bristol University, Bristol, U.K. [b] Physical Chemistry Laboratory, Oxford, U.K.

To cite this Article Bartlett, P. and Howard, B. J.(1990) 'The rotational-vibrational spectrum of symmetric non-rigid triatomics in hyperspherical coordinates: the H^+_3 molecule', Molecular Physics, 70: 6, 1001 — 1029
To link to this Article: DOI: 10.1080/00268979000101491
URL: http://dx.doi.org/10.1080/00268979000101491

MOLECULAR PHYSICS, 1990, VOL. 70, NO. 6, 1001–1029

The rotational–vibrational spectrum of symmetric non-rigid triatomics in hyperspherical coordinates: the H_3^+ molecule

By P. BARTLETT
School of Chemistry, Cantocks Close, Bristol University, Bristol BS8 1TS, U.K.
and B. J. HOWARD
Physical Chemistry Laboratory, South Parks Road, Oxford University, Oxford OX1 3QZ, U.K.

(*Received 7 March 1990; accepted 18 April 1990*)

Theoretical methods are described for the calculation of rovibrational levels of symmetric non-rigid triatomics using the symmetric hyperspherical coordinates of Smith and Whitten. An adiabatic separation of radial and angular motion is shown to be valid for H_3^+. The adiabatic angular functions are chosen as a linear combination of products of angular-momentum eigenfunctions and specially developed hyperspherical basis functions. Corrections to the adiabatic approximation are included by Brillouin–Wigner perturbation theory. Results are given for the H_3^+ system. The present approach has the advantage that all symmetric arrangements are treated equivalently.

1. Introduction

In the last few years significant progress has been made in the theoretical treatment of large-amplitude motion in small molecules. For near-rigid molecules the most widely used choice of coordinates originates from the work of Eckart [1]. In this approach it is assumed that the potential-energy surface defines an equilibrium nuclear geometry. However, it is widely recognized that the Eckart embedding of the body-fixed (BF) axes is unsuitable for molecules with large-amplitude motions. The difficulty is easily seen by considering the case of a triatomic molecule in which a large-amplitude vibrational motion distorts the molecule into a linear geometry. The instantaneous moment-of-inertia tensor has a zero diagonal element, its inverse is singular, and hence the Eckart Hamiltonian is undefined. This apparent singularity arises because it is not possible to define all three Euler angles uniquely for a collinear arrangement of atoms. Consequently, the domain of the Eckart Hamiltonian is restricted to those functions that vanish sufficiently rapidly close to the linear geometry so that the matrix elements of the internal Hamiltonian converge [2]. Although the singularity in the kinetic-energy operator may always be avoided by, for example, arbitrarily confining trial functions [3], the accuracy of this approach is questionable if the molecular potential does not exclude collinear geometries. The treatment of large-amplitude motion in highly symmetric molecules is further complicated by the Eckart fixing of the body-fixed axes to the equilibrium geometry. Each symmetry operation requires the setting up of a new Eckart axis system, with a consequent redefinition of the Euler angles. This leads to considerable difficulty in constructing trial functions with the full permutational symmetry.

Several new techniques have been developed for the calculation of vibrational–rotational levels that avoid some of the problems associated with the Eckart embedding of the BF axes. In particular, Tennyson and Sutcliffe [4, 5], in calculations on

0026-8976/90 $3.00

systems as diverse as KCN and HeHF, have used Jacobi (atom–diatom) coordinates with a BF z axis aligned along the collision coordinate. In these coordinates the Hamiltonian is sufficiently simple that large-amplitude internal motion may be completely described. A careful choice for the asymptotic form of basis functions ensures the apparent singularity associated with the linear geometry does not cause any numerical problems. This approach has been applied to the symmetric oblate top H_3^+ [6], although accurate calculations required very large basis set expansions. The slow convergence of these calculations reflects two difficulties with the use of Jacobi coordinates. First, the operations of the molecular symmetry group D_{3h} produce a complicated mixture of Jacobi coordinates, which makes it very difficult to define basis functions with the full permutational symmetry. Consequently, calculations have been limited to using a partially symmetrized basis set, with the result that large numbers of basis functions are required for a good representation. Secondly, the use of an in-plane BF z axis couples all the different BF angular-momenta components together, leading to a set of strongly coupled rotational states. Any realistic calculation for H_3^+ in Jacobi coordinates must include all off-diagonal Coriolis and asymmetric-top interactions. No simplifying rotational-decoupling approximation is appropriate. The size of this full rovibrational calculation increases linearly with the value of the total angular momentum J and soon becomes intractable. Fully coupled calculations have consequently been limited to low-J states, typically $J \leqslant 4$ [6], although Tennyson and Sutcliffe [7] have proposed a two-step variational procedure for the calculation of highly excited rotational states of H_3^+ and its isomers.

In symmetric molecules, large-amplitude motion is more efficiently treated using a symmetrised set of coordinates in which all symmetric arrangements are treated equivalently. Some time ago, Smith and Whitten (SW) [8] developed a system of hyperspherical coordinates in which atomic permutation is accomplished simply by adding a constant phase angle to one of the angular coordinates. Apart from this phase-angle difference, the internal coordinates are unaffected by permutation. It is therefore relatively easy to generate basis sets that transform as one of the irreducible representations of D_{3h}. A very clear description of the properties of this coordinate system has been given by Johnson [9]. For calculations of large-amplitude motions in symmetric oblate tops such as H_3^+, the SW hyperspherical system has several advantages when compared with Jacobi coordinate systems. First, the full molecular symmetry may be used to reduce the size of any calculation. Secondly, there is a unique radial coordinate ρ that is invariant under all symmetry operations. Motion along the radial coordinate may therefore be formally separated from motion in the angular coordinates. With an adiabatic assumption, the internal eigenstates are expressed as a product of the solution of a five-dimensional equation (two internal and three rotational degrees of freedom) and a set of coupled radial equations. The usefulness of this approach depends upon the strength of the non-adiabatic radial-coupling terms. In the molecular systems so far considered [10] the radial coupling was sufficiently small that the correction terms could be accurately included by a perturbation treatment. The adiabatic separation, which is possible in a hyperspherical (but not in a Jacobi) coordinate system, reduces the maximum dimension of the matrix equations that must be solved, leading to a considerable saving in computational effort. Thirdly, the SW coordinate system is an instantaneous principal-axis system, with the BF z axis directed along the symmetry axis of the oblate top. This choice minimizes the off-diagonal coupling between states of

different BF z component of angular momentum, and suggests that an angular-momentum decoupling approximation, analogous to the centrifugal sudden approximation [11] used in inelastic scattering, may be useful. This promises to reduce significantly the amount of computer time required to calculate high rotational states.

The triatomic molecular ion H_3^+ is one of the simplest known polyatomic molecules and has been the subject of many theoretical and experimental investigations. Because of its light mass, large-amplitude internal motion is important, even at relatively low energies. That this is so can be seen from the potential-energy surface of Schinke, Dupuis and Lester (SDL) for the ground electronic state $^1A_1'$ [12]. The minimum-energy configuration corresponds to an equilateral triangle (oblate symmetric top). Yet at energies of about 13 000 cm^{-1} above the potential minimum, H_3^+ may become collinear (prolate symmetric top). The flatness of the potential at these energies results in very-large-amplitude internal motion in which the system can access all possible triangular and collinear geometries so that permutation of the hydrogen nuclei is a facile process. With increasing energy, the H_3^+ system becomes localised at obtuse isoscelles configurations, with hindered internal rotation of the diatomic, analogous to a van der Waals atom–diatom complex. At an energy of about 39 000 cm^{-1} the molecular ion dissociates into $H_2(^1\Sigma_g^+)$ and H^+. For comparison, the calculated zero-point energy for H_3^+ on this surface is about 4330 cm^{-1}. Large-amplitude motion is therefore expected to be important in H_3^+, even at low degrees of vibrational excitation. As a result of the simplicity of the H_3^+ ion, several very accurate *ab initio* potential-energy surfaces are available [12–15]. Calculations on H_3^+ should therefore provide a benchmark by which to compare different approaches to the treatment of large-amplitude motions in non-rigid molecules.

The first and most extensive calculation of the rotational–vibrational spectra of H_3^+ was made by Carney and Porter [13, 16, 17]. Vibrational energies and wavefunctions were calculated by expanding Watson's form of the Eckart Hamiltonian for nonlinear molecules in a basis set of 220 harmonic-oscillator product functions. These calculations concentrated on the low-lying vibrational states. The higher vibrational–rotational states have been more accurately converged in the calculations of Tennyson and Sutcliffe [6]. In this study the basis functions were not adapted to the full symmetry group of D_{3h}, but a large set of basis functions (880 functions for $J = 0$ calculations) was used in order to ensure convergence to at least 1 cm^{-1} or better. In recent calculations [15, 18–20] the availability of more accurate potential-energy surfaces has improved the agreement between the calculated fundamental vibrational frequencies and the experimentally derived values.

Previous calculations using hyperspherical coordinates of the bound-state dynamics of triatomics have been limited to the purely vibrational eigenstates. Frey and Howard [10, 21] have calculated the vibrational levels of inert-gas and molecular-hydrogen trimers by expanding the angular wavefunction in hyperspherical harmonics. These functions are eigenfunctions of the kinetic-energy operator and therefore have the correct asymptotic behaviour at the symmetric-top singularity present in the $J = 0$ Hamiltonian. However, in bound states of a molecular system, where the potential energy is comparable to the kinetic energy, a large basis set of hyperspherical harmonics is necessary for adequate convergence. Additionally, there are difficulties in extending this approach to states with non-zero J since the angular basis functions must also have a defined asymptotic behaviour at the collinear geometry where the internal Hamiltonian for $J \neq 0$ is undefined.

Closed analytic expressions for the hyperspherical harmonics for non-zero total angular momentum are unknown.

Hyperspherical coordinates have also been used in a recent calculation of the vibrational eigenstates of H_3^+ [22]. A product basis set of one dimensional functions together with successive diagonalisation and truncation was used to generate accurate vibrational levels. An alternative body-fixed hyperspherical coordinate system [23] was used. This differs principally from the present hyperspherical system in that the BF z axis is defined in the plane of the particles. This choice is better for systems dominated by near-linear configurations. For zero-angular-momentum states, Whitnall and Light developed a method to handle the singularity in the Hamiltonian at the symmetric-top configuration. However, for states with a non-zero angular momentum, the Hamiltonian has an additional singular off-diagonal Coriolis term at the symmetric-top configuration. As a result, the approach of Whitnall and Light cannot be applied to non-zero-J states.

In this article we present an accurate calculation of the vibrational–rotational eigenvalues of H_3^+ using the hyperspherical coordinates introduced by Smith and Whitten. In the next section we discuss the coordinate system used in this work, its symmetry properties, and the form of the molecular Hamiltonian. The orientation of the body-fixed axes is labelled by three Euler angles, while the internal radial coordinate ρ describes the overall size of the molecular system and the angular coordinates (ϑ, φ) describe its shape. To aid in visualising the molecular motion in hyperspherical coordinates, we describe a stereographic projection of the H_3^+ potential at fixed ρ. We assume that motion along the radial coordinate may, as an initial approximation, be adiabatically separated from motion in the angular coordinates. In section 3 we describe the expansion of the full wavefunction in a set of adiabatic surface functions which are parametric functions of ρ. We choose the adiabatic surface functions as solutions of a fixed-ρ angular Hamiltonian. In section 4 we discuss the basis functions used to diagonalise this angular Hamiltonian and their symmetry adaption. The full molecular symmetry is used to reduce the size of the present calculation. In section 5 we give a description of our method for obtaining the adiabatic surface functions. Section 6 gives the resulting coupled-channel radial equations and describes their solution, in the limit of weak coupling, by an iterative form of Brillouin–Wigner perturbation theory. Section 7 contains the results of our rovibrational calculations on H_3^+ and section 8 gives our conclusions.

2. Hyperspherical coordinates and the molecular Hamiltonian

The hyperspherical coordinate system of Smith and Whitten [8] has been described in detail by Johnson [9], so we give here only the details necessary to understand our calculations.

The hyperspherical coordinates are defined in terms of the mass-scaled [24] Jacobi vectors $\mathbf{r}^k$ and $\mathbf{R}^k$, where $\mathbf{r}^k$ is the scaled vector from atom i to atom j and $\mathbf{R}^k$ is the scaled vector from the centre of mass of diatomic ij to atom k. The hyperspherical coordinates divide into two sets: the internal coordinates $(\rho, \vartheta, \varphi)$, which determine the size and shape of the triangle formed by the Jacobi vectors, and the external coordinates (α, β, γ), which specify the orientation of the BF axis system. The Euler angles are chosen so that the BF z axis points in the direction of the vector product $\mathbf{r}^k \times \mathbf{R}^k$ while the BF y axis is parallel to the larger of the two in-plane instantaneous moments of inertia, with an absolute sense determined by the

set of internal coordinates $(\rho, \vartheta, \varphi)$. The BF axes are a system of instantaneous principal axes in which the moment-of-inertia tensor is diagonal, with the elements

$$\left.\begin{aligned} I_{xx} &= \mu\rho^2 \sin^2 \vartheta, \\ I_{yy} &= \mu\rho^2 \cos^2 \vartheta, \\ I_{zz} &= \mu\rho^2, \end{aligned}\right\} \tag{1}$$

such that $I_{zz} \geqslant I_{yy} \geqslant I_{xx}$. Only for molecular configurations with the equilibrium geometry are the hyperspherical body fixed axes (x, y, z) identical with the conventionally defined Eckart principal axes (a, b, c). As the molecule vibrates, the hyperspherical axes rotate smoothly, following the intantaneous axes of inertia, in contrast with the behaviour of the Eckart axes, which are fixed by the equilibrium molecular geometry. The three internal coordinates are defined by the components of the mass-scaled Jacobi vectors in the BF axis system, namely

$$\left.\begin{aligned} r_x^k &= \rho \cos \vartheta \cos \varphi, \\ r_y^k &= -\rho \sin \vartheta \sin \varphi, \\ R_x^k &= \rho \cos \vartheta \sin \varphi, \\ R_y^k &= \rho \sin \vartheta \cos \varphi, \end{aligned}\right\} \tag{2}$$

with coordinate ranges

$$0 \leqslant \rho \leqslant \infty, \qquad 0 \leqslant \vartheta \leqslant \tfrac{1}{4}\pi, \qquad 0 \leqslant \varphi \leqslant 2\pi, \tag{3}$$

and a volume element

$$\mathrm{d}v' = \tfrac{1}{4}\rho^5 \sin 4\vartheta \sin \beta \, \mathrm{d}\rho \, \mathrm{d}\vartheta \, \mathrm{d}\varphi \, \mathrm{d}\alpha \, \mathrm{d}\beta \, \mathrm{d}\gamma. \tag{4}$$

The range of φ spans configuration space twice since the two sets of coordinates $(\rho, \vartheta, \varphi, \alpha, \beta, \gamma)$ and $(\rho, \vartheta, \varphi + \pi, \alpha, \beta, \gamma + \pi)$ refer to the same physical arrangement of particles but referenced to the two possible BF axis systems, which differ only in the absolute sense of the x and y axes. This duplication ensures the motion of the instantaneous BF axis system is always continuous and, as shown by Pack and Parker [23], avoids discontinuous half-integral angular-momentum functions of φ.

The Hamiltonian operator in hyperspherical coordinates is [25]

$$\begin{aligned} H' = &-\frac{\hbar^2}{2\mu}\frac{1}{\rho^5}\frac{\partial}{\partial\rho}\rho^5\frac{\partial}{\partial\rho} - \frac{\hbar^2}{2\mu\rho^2}\left[\frac{1}{\sin 4\vartheta}\frac{\partial}{\partial\vartheta}\sin 4\vartheta\frac{\partial}{\partial\vartheta} + \frac{1}{\cos^2 2\vartheta}\frac{\partial^2}{\partial\varphi^2}\right] \\ &+ AJ_x^2 + BJ_y^2 + CJ_z^2 - \frac{\mathrm{i}\hbar^2 \sin 2\vartheta}{\mu\rho^2 \cos^2 2\vartheta} J_z \frac{\partial}{\partial\varphi} + V(\rho, \vartheta, \varphi), \end{aligned} \tag{5}$$

where the J_i $(i = x, y \text{ or } z)$ are the BF components of the total-angular-momentum operator (in units of $\hbar$),

$$A = \hbar^2/(2\mu\rho^2 \sin^2 \vartheta), \qquad B = \hbar^2/(2\mu\rho^2 \cos^2 \vartheta), \qquad C = \hbar^2/(2\mu\rho^2 \cos^2 2\vartheta),$$

and μ is the three-body reduced mass $(\mu^2 = m_1 m_2 m_3/(m_1 + m_2 + m_3))$. We note, following (3), that the 'rotational constants' A, B and C satisfy the inequalities $A \geqslant B$ and $C \geqslant B$. It is convenient to rewrite (5) in the form

$$H' = T_{\rho'} + T_a + T_r + T_c + V(\rho, \vartheta, \varphi) \tag{6}$$

where each consecutive line of (5) is identified with the terms above: T_ρ, the radial (ρ), T_a the angular (ϑ, φ), T_r the rotational, T_c the Coriolis kinetic-energy operators and $V(\rho, \vartheta, \varphi)$ the molecular potential. In the later discussion we shall find it useful to subdivide the rotational kinetic-energy operator T_r into the symmetric-top portion

$$T_{sym} = \tfrac{1}{2}(A + B)(J^2 - J_z^2) + CJ_z^2 \tag{7}$$

and the (remaining) asymmetric-top portion

$$T_{asy} = \tfrac{1}{2}(A - B)(J_x^2 - J_y^2). \tag{8}$$

We note that T_r is not the normal asymmetric-rotor kinetic-energy operator since, although $A = \hbar^2/2I_{xx}$ and $B = \hbar^2/2I_{yy}$, $C \neq \hbar^2/2I_{zz}$. Similarly, the 'rotational constants' defined above do not follow the expected order $A \geqslant B \geqslant C$. Eckart [26] showed that such anomalous 'rotational constants' are a consequence of using a BF instantaneous principal-axis system. In such a system the Coriolis terms, describing the interaction between rotational and vibrational motions, are of a larger order of magnitude than those due to rotation alone. If the off-diagonal Coriolis terms are included into a diagonal effective kinetic-energy operator then, as Van Vleck [27] showed, the usual rigid-rotor expression is obtained for the purely rotational term. In later work Eckart [1] abandoned the instantaneous-axis system in favour of fixing the molecular axes by the equilibrium moments of inertia. This choice minimises the magnitude of the Coriolis terms.

The Schrödinger equation may be transformed in order to simplify the differential terms in ρ. On defining the transformed wavefunction ψ as

$$\psi = \rho^{5/2}\Psi, \tag{9}$$

where Ψ is an eigenfunction of the untransformed Hamiltonian operator H', (5), the Schrödinger equation for ψ becomes

$$H\psi = E\psi, \tag{10}$$

where the transformed Hamiltonian operator is given by

$$H = \rho^{5/2}H'\rho^{-5/2}. \tag{11}$$

After this transformation, the Hamiltonian operator may be written as

$$H = T_\rho + T_a + T_r + T_c + V(\rho, \vartheta, \varphi), \tag{12}$$

where

$$T_\rho = -\frac{\hbar^2}{2\mu}\left(\frac{\partial^2}{\partial\rho^2} - \frac{15}{4\rho^2}\right)$$

and T_a, T_r and T_c are as in (5). The transformed volume element is

$$d\nu = \tfrac{1}{4} \sin 4\vartheta \sin\beta \, d\rho \, d\vartheta \, d\varphi \, d\alpha \, d\beta \, d\gamma. \tag{13}$$

This Hamiltonian is the one used in the remainder of this paper.

The rotational–vibrational levels of H_3^+ may be labelled according to the irreducible representations of D_{3h}, which is isomorphic with $S_3 \times \{E, E^*\}$. The effects of the permutation–inversion operators of D_{3h} are easily derived using the defini-

tions above and those given by Johnson [9]. In the representation of the symmetric group S_3 a passive convention is used in which atomic labels rather than atomic coordinates are permuted.

The external coordinates (α, β, γ) are unaffected by the operators **E**, **(123)** and **(132)**, while the pairwise permutation **(*ij*)** is equivalent to a rotation of π about the BF y axis:

$$(ij)\begin{bmatrix}\alpha\\ \beta\\ \gamma\end{bmatrix} = \begin{bmatrix}\pi+\alpha\\ \pi-\beta\\ \pi-\gamma\end{bmatrix}. \tag{14}$$

The space-fixed inversion operator **E*** is equivalent to a rotation of π about the BF z axis and a change in the sense of all axes:

$$\mathbf{E}^*\begin{bmatrix}\alpha\\ \beta\\ \gamma\end{bmatrix} = \begin{bmatrix}\alpha\\ \beta\\ \gamma+\pi\end{bmatrix}. \tag{15}$$

The internal coordinates (ρ, ϑ) are unaffected by any of the operators of D_{3h}, while the kinematic angle φ exhibits the following behaviour.

$$\left.\begin{aligned}(12)\varphi &= -\varphi,\\ (13)\varphi &= -\varphi - \tfrac{4}{3}\pi,\\ (23)\varphi &= -\varphi + \tfrac{4}{3}\pi,\\ (123)\varphi &= \varphi + \tfrac{4}{3}\pi,\\ \mathbf{E}^*\varphi &= \varphi.\end{aligned}\right\} \tag{16}$$

In hyperspherical coordinates $\vartheta = \frac{1}{4}\pi$ describes equilateral triangular configurations, while for $\vartheta = 0$ the three atoms are collinear. The angular dependence of the molecular potential at fixed ρ may be visualised by using a stereographic projection of the upper surface of the sphere covered by the spherical polar coordinates $\vartheta' = \frac{1}{2}\pi - 2\vartheta$ and $\varphi' = 2\pi - 2\varphi$. A point in this plot with Cartesian coordinates x and y corresponds to the internal configuration (ϑ, φ), where

$$\left.\begin{aligned}x &= \tan(\tfrac{1}{4}\pi - \vartheta)\cos 2\varphi,\\ y &= -\tan(\tfrac{1}{4}\pi - \vartheta)\sin 2\varphi.\end{aligned}\right\} \tag{17}$$

There is only one point on the projected plot corresponding to each internal configuration so the mapping is unique. Furthermore, each molecular permutation is equivalent to a rotation of the plot about the z axis without distortion.

Stereographic projections of the H_3^+ potential of Schinke, Dupuis and Lester at three fixed values of ρ are shown in figure 1. The dashed circles show curves of constant ϑ at 5° intervals, with the central point on the projection corresponding to the equilateral triangle configuration $\vartheta = \frac{1}{4}\pi$. In figure 1 (*a*) the angular form of the potential is shown at $\rho = 1{\cdot}2$ Å, close to the absolute minimum in the potential ($\rho = 1{\cdot}151$ Å, $\vartheta = \frac{1}{4}\pi$). Motion along the contours is approximately parallel to φ, while motion perpendicular to the contours is approximately parallel to ϑ. It is clear that at small ρ the motions along the internal coordinates ϑ and φ are largely separable. In fact, at $\vartheta = \frac{1}{4}\pi$, ϑ and φ are totally separable, since for an equilateral

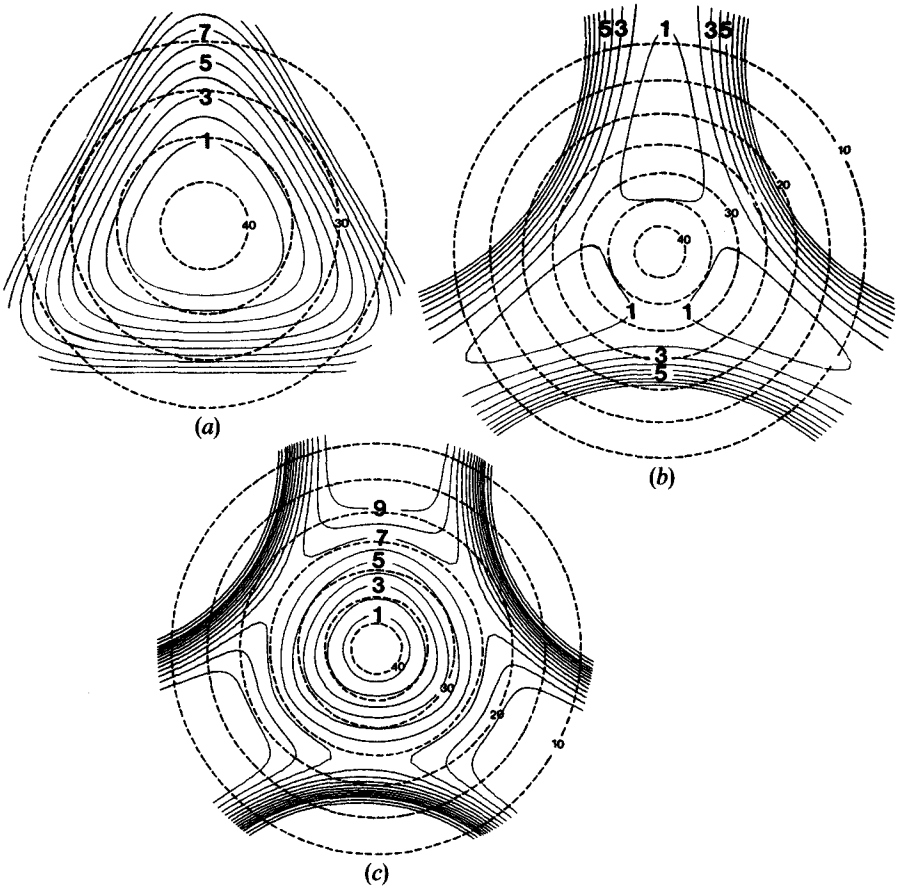

Figure 1. Stereographic projections of the H_3^+ potential of Schinke *et al.* [12] at $\rho = 1{\cdot}2$ Å (*a*), 1·7 Å (*b*) and 2·0 Å (*c*). The solid contours are at intervals of 1000 cm^{-1} in (*a*) and (*b*), and 500 cm^{-1} in (*c*). The lowest contour corresponds to potential energies of 2000 cm^{-1} (*a*), 14 000 cm^{-1} (*b*) and 22 500 cm^{-1} (*c*) above the potential minimum. The broken circles depict lines of constant ϑ, in 5° intervals, with the equilateral geometry ($\vartheta = 45°$) at the centre of the projection.

geometry all axes in the plane of the atoms are principal axes of inertia. Motion in φ is equivalent to a rotation about the BF z axis, while motion in ϑ corresponds to an internal vibration. At $\rho = 1{\cdot}7$ Å the potential surface shows three symmetric angular minima at obtuse isocelles geometries separated by saddle points at acute isocelles geometries. At $\rho = 2{\cdot}0$ Å the angular minima has shifted to still smaller values of ϑ and the barrier to interconversion has increased considerably. Within each of the three channels, motion parallel to the contours describes hindered rotation of the diatomic in the atom–diatom complex, while motion perpendicular to the contours is largely vibration of the diatomic. At large ρ, as the plot of figure 1 (*c*) shows, motion along the internal angular coordinates ϑ and φ is strongly coupled.

3. The wavefunction in hyperspherical coordinates

Without loss of generality, the eigenfunctions of the transformed Hamiltonian (12), for a given total angular momentum J, M (space-fixed component of J) and

symmetry Γ, may be expanded in the form

$$\psi^{JM\Gamma} = \sum_{t}^{N_t} \chi_t^{J\Gamma}(\rho)\Phi_t^{JM\Gamma}(\Omega; \rho), \tag{18}$$

where Ω refers to the set of angular coordinates $(\alpha, \beta, \gamma, \vartheta, \varphi)$ and the functions Φ depend parametrically upon the radial coordinate ρ. Implicit in this expansion is the belief that only a few adiabatic states t need be considered for a good description of nonlinear triatomics such as H_3^+. This assumption is considered in greater detail in section 6. We choose the adiabatic surface functions Φ, used as basis functions here, as solutions of the five-dimensional Schrödinger equation in the internal coordinates (ϑ, φ) and the Euler angles (α, β, γ):

$$\left[T_a + T_r + T_c + \frac{15\hbar^2}{8\mu\rho^2} + V(\rho, \vartheta, \varphi)\right]\Phi_t^{JM\Gamma}(\Omega; \rho) = U_t^{J\Gamma}(\rho)\Phi_t^{JM\Gamma}(\Omega; \rho), \tag{19}$$

where the kinetic energy and the molecular potential are evaluated at a fixed radial value ρ. Here T_a is the internal angular (ϑ, φ) kinetic energy, T_r is the rotational kinetic energy and T_c the Coriolis terms defined in (12) and (5). As we shall show in section 4, the solutions to (19) may be written in the form

$$\Phi_t^{JM\Gamma}(\Omega; \rho) = \sum_{kvm} c_{kvm}^{J\Gamma t}(\rho)\hat{Y}_{kvm}^{JM\Gamma}(\Omega), \tag{20}$$

where the symmetrised angular basis functions are given by

$$\hat{Y}_{kvm}^{JM\Gamma}(\Omega) = \frac{1}{4\pi}\left[\frac{2J+1}{2\pi(1+\delta_{k0})}\right]^{1/2} f_{kvm}^{J}(\vartheta) \times [D_{Mk}^{J*}(\alpha, \beta, \gamma)e^{-iv\varphi} + (-1)^{J+k+\sigma}D_{M-k}^{J*}(\alpha, \beta, \gamma)e^{iv\varphi}]. \tag{21}$$

In the expansion (20) the values of the angular-momentum quantum number k and the kinematic quantum number v are restricted by the state symmetry Γ. In (21), D_{Mk}^{J*} is the unnormalised Wigner D matrix, defined following the conventions of Brink and Satchler [28], f_{kvm}^{J} is the normalised ϑ function introduced in the next section and $c_{kvm}^{J\Gamma t}(\rho)$ are the expansion coefficients.

The angular surface function $\Phi(\Omega; \rho)$ transforms as one of the irreducible representation Γ of the molecular symmetry group D_{3h}. This group is generated by the operators for space-fixed inversion **E***, pairwise permutation (**12**) and cyclic permutation (**123**). From the fact that the space-fixed inversion operator **E*** only affects γ, and using (15), we immediately have that the angular basis function $\hat{Y}(\Omega)$, defined in (21), has the following simple symmetry under inversion:

$$\mathbf{E}^*\hat{Y}_{kvm}^{JM\Gamma}(\Omega) = (-1)^k\hat{Y}_{kvm}^{JM\Gamma}(\Omega). \tag{22}$$

Hence for surface functions Φ of definite parity the k sum in (20) is restricted to either all-odd or all-even values of k. Furthermore, the twofold mapping of configuration space, discussed in section 2, leads to the equality

$$\hat{Y}_{kvm}^{JM\Gamma}(\alpha, \beta, \gamma, \vartheta, \varphi) = \hat{Y}_{kvm}^{JM\Gamma}(\alpha, \beta, \gamma + \pi, \vartheta, \varphi + \pi), \tag{23}$$

so that k and v in the sum (20) must be both even or both odd, depending on the parity of the surface function Φ.

To see the effect of the pairwise permutation, we note from (14) that (**12**) takes $D_{Mk}^{J*}(\alpha, \beta, \gamma)$ into

$$D_{Mk}^{J*}(\alpha + \pi, \pi - \beta, \pi - \gamma) = (-1)^{J+k}D_{M-k}^{J*}(\alpha, \beta, \gamma). \tag{24}$$

Table 1. The set of angular basis functions of angular-momentum projection k (e/o labels the parity of k and σ) and symmetry species Γ. For non-zero k, v is restricted to the values $\pm[v]$, while for $k = 0$, v may have any one of the set of values $[v]$. The symmetry of the basis function under pairwise permutation is labelled by σ.

Irreducible representation Γ	Parity of σ	Parity of k	$[v]$ $n = 0, 1, 2, \ldots$
A_1'	e	e	$6n$
A_1''	e	o	$3 + 6n$
A_2'	o	e	$6n$
A_2''	o	o	$3 + 6n$
E'	e/o	e	$2 \pm 6n$
E''	e/o	o	$1 \pm 6n$

Together with the transformation properties of φ, given by (16), pairwise permutation transforms the product $f^J_{kvm}(\vartheta)D^{J*}_{Mk}(\alpha, \beta, \gamma)e^{-iv\varphi}$ as

$$(\mathbf{12})f^J_{kvm}(\vartheta)D^{J*}_{Mk}(\alpha, \beta, \gamma)e^{-iv\varphi} = (-1)^{J+k}f^{J*}_{kvm}(\vartheta)D^{J*}_{m-k}(\alpha, \beta, \gamma)e^{iv\varphi}. \quad (25)$$

The range of k in (20) may therefore be further restricted to non-negative values. For $k \geqslant 1$, the basis functions $\hat{Y}_{kvm}$ and $\hat{Y}_{k-vm}$ are different and in general both functions must be included in the sum (20). For the particular case of $k = 0$, the two functions differ only by a phase factor and the summation in (20) may be further restricted to positive quantum numbers. The symmetrised angular basis functions transform with the character $(-1)^\sigma$ under pairwise permutation.

Under the cyclic permutation (**123**), the only coordinate affected is the kinematic angle φ which transforms into $\varphi + \frac{4}{3}\pi$. Hence angular functions $\hat{Y}^{JM\Gamma}_{kvm}(\Omega)$ with v a multiple of three are unaffected by the cyclic permutation (**123**) and transform as one of the two one-dimensional irreducible representations of S_3, depending on the sign of $(-1)^\sigma$. Angular basis functions where v is not a multiple of three form a representation of the two-dimensional irreducible representation of S_3. Combining the transformation properties of the angular basis functions, table 1 shows the restrictions on the quantum numbers k and v in the summation in (20) for surface functions Φ that transform as the irreducible representation Γ of D_{3h}.

4. Adiabatic surface functions: choice of basis set

The adiabatic surface functions $\Phi(\Omega; \rho)$, which depend parametrically upon ρ, are solutions to the Schrödinger equation (19) where the effective angular potential is the molecular potential $V(\rho, \vartheta, \varphi)$ evaluated at fixed ρ. As is readily seen from figure 1 (*a*), the H_3^+ angular potential at small ρ is almost independent of φ so that (19) is approximately separable. With an increase in ρ, figure 1 (*c*) shows the angular minimum shifts from the equilateral geometry at $\vartheta = \frac{1}{4}\pi$ to a near-collinear configuration of $\vartheta \approx 0$ as the atom–diatom dissociation limit is approached. At these large values of ρ, the motion in the ϑ and φ coordinates is strongly coupled and (19) is highly non-separable. Because of the large change in the nature of the adiabatic solutions $\Phi(\Omega; \rho)$ with ρ, it is very difficult to choose a basis set that will be useful at all values of ρ. We shall, however, restrict attention to the low-lying states of H_3^+, where the near-collinear geometry ($\vartheta \approx 0$) is not significant. We seek

an expansion of the adiabatic surface functions $\Phi(\Omega; \rho)$ in a set of symmetrised basis functions $\hat{Y}(\Omega)$, which we choose as eigenfunctions of the fixed-ρ Hamiltonian H_0 given by

$$H_0 = T_a + T_r + T_c + \frac{15\hbar^2}{8\mu\rho^2} + V_0(\rho, \vartheta), \tag{26}$$

where the kinetic-energy terms are identical with those of (19) and the reference potential V_0 has the simple form

$$\frac{2\mu\rho^2}{\hbar^2} V_0(\rho, \vartheta) = \Delta + 4\xi^2 \cos^2 2\vartheta. \tag{27}$$

The angular potential V_0 (at fixed ρ) has a minimum at $\vartheta = \frac{1}{4}\pi$ and is independent of φ. With increasing ξ, the wavefunction is localised at $\vartheta = \frac{1}{4}\pi$. The similarity of the small-ρ H_3^+ potential and the reference potential V_0 ensures that only a few terms need be considered in the surface wavefunction expansion (20). At larger ρ, as the amplitude of the wavefunction at $\vartheta = 0$ increases, the convergence is expected to be slower.

With increasing ξ, the basis functions $\hat{Y}(\Omega)$ are localised near $\vartheta = \frac{1}{4}\pi$. To consider behaviour of the basis function $\hat{Y}(\Omega)$ at ϑ near $\frac{1}{4}\pi$, we rewrite the kinetic-energy portion of (26) as

$$T_i = -\frac{\hbar^2}{2\mu\rho^2}\left[\frac{1}{\sin 4\vartheta}\frac{\partial}{\partial\vartheta}\sin 4\vartheta\frac{\partial}{\partial\vartheta} + \frac{1}{\cos^2 2\vartheta}\frac{\partial^2}{\partial\varphi^2}\right] + \tfrac{1}{2}(A + B)(J^2 - J_z^2)$$
$$+ CJ_z^2 + \tfrac{1}{2}(A - B)(J_x^2 - J_y^2) - \frac{i\hbar^2 \sin 2\vartheta}{\mu\rho^2 \cos^2 2\vartheta} J_z \frac{\partial}{\partial\varphi}, \tag{28}$$

where $T_i = T_a + T_r + T_c$. Here the coefficient of the asymmetric-rotor-like term is

$$\tfrac{1}{2}(A - B) = \frac{\hbar^2}{4\mu\rho^2}\left(\frac{1}{\sin^2\vartheta} - \frac{1}{\cos^2\vartheta}\right) = \frac{\hbar^2}{\mu\rho^2}\frac{\cos 2\vartheta}{\sin^2 2\vartheta}. \tag{29}$$

For $\vartheta \approx \frac{1}{4}\pi$ this last term becomes small and we shall neglect it in deriving the form of the basis functions. In this limit there is no coupling between the different components of the angular momentum along the BF z axis. Note, however, that at the collinear geometry ($\vartheta \approx 0$) this term is divergent. The angular momentum J is now coupled to the BF x axis, and all possible components $-J \leqslant k \leqslant J$ of the angular momentum along the BF z axis, consistent with the molecular parity, are strongly mixed. In such a case the present embedding of the body-fixed axes is inappropriate and it is much simpler to redefine the BF z axis so it lies in the molecular plane.

The reference potential $V_0(\rho, \vartheta)$ is independent of φ, and consequently the Schrödinger equation corresponding to the Hamiltonian operator H_0 (neglecting the asymmetric rotor terms of (28) and (29)) is separable. The unsymmetrised solutions may be written as

$$Y_{kvm}^{JM}(\Omega) = \frac{1}{4\pi}\left(\frac{2J+1}{\pi}\right)^{1/2} f_{kvm}^{J}(\vartheta) D_{Mk}^{J*}(\alpha, \beta, \gamma) e^{-iv\varphi}, \tag{30}$$

where v is the eigenvalue of the kinematic angular-momentum operator $-i\,\partial/\partial\varphi$, and the rotation matrix $[(2J+1)^{1/2}/4\pi]D_{Mk}^{J*}$ is the normalised symmetric-top wavefunction for total angular-momentum quantum number J with components k and M along the BF and SF z axes respectively. Substitution of the wavefunction

expansion (30) into the Schrödinger equation for the Hamiltonian operator (26) gives the following equation for the functions f:

$$\left\{-\frac{\hbar^2}{2\mu\rho^2}\frac{1}{\sin 4\vartheta}\frac{\mathrm{d}}{\mathrm{d}\vartheta}\sin 4\vartheta\frac{\mathrm{d}}{\mathrm{d}\vartheta}+\frac{\hbar^2}{2\mu\rho^2\cos^2 2\vartheta}(v^2+k^2-2kv\sin 2\vartheta)\right.$$
$$\left.+\frac{\hbar^2}{\mu\rho^2\sin^2 2\vartheta}[J(J+1)-k^2]+V_0(\rho,\vartheta)-E^J_{kvm}(\rho)\right\}f^J_{kvm}(\vartheta)=0. \quad (31)$$

The effective angular potential in (31) is singular at both the equilateral ($\vartheta=\frac{1}{4}\pi$) and collinear ($\vartheta=0$) configurations. Since the eigenvalues of the Hamiltonian operator (26) must remain finite for wavefunctions localised either at $\vartheta=\frac{1}{4}\pi$ or $\vartheta=0$, the asymptotic forms of valid solutions are determined by the singularities in the effective-potential terms. For ϑ near $\frac{1}{4}\pi$ (31) may be approximated by

$$\left\{-\frac{\hbar^2}{2\mu\rho^2}\left[\frac{1}{\sin 4\vartheta}\frac{\mathrm{d}}{\mathrm{d}\vartheta}\sin 4\vartheta\frac{\mathrm{d}}{\mathrm{d}\vartheta}-\frac{(v-k)^2}{\cos^2 2\vartheta}+n^J_{kvm}\right]\right\}_{\vartheta\to\pi/4} f^J_{kvm}(\vartheta)=0, \quad (32)$$

where only the divergent terms have been retained. Equation (32) is simply solved and the $\vartheta=\frac{1}{4}\pi$ asymptotic limit of the function $f(\vartheta)$ is given by

$$f^J_{kvm}(\vartheta)\sim\cos^p 2\vartheta\, P_m^{(0,p)}(\cos 4\vartheta) \quad \text{as} \quad \vartheta\to\tfrac{1}{4}\pi, \quad (33)$$

where the index $p=|\frac{1}{2}(v-k)|$ and $P_m^{(0,p)}$ is a Jacobi polynomial [29] of degree m. The eigenvalue n^J_{kvm} is given by

$$n^J_{kvm}=(4m+|v-k|)(4m+|v-k|+4). \quad (34)$$

Similarly, in the limit of small ϑ the asymptotic form of the function $f(\vartheta)$ is the solution of the equation

$$\left\{-\frac{\hbar^2}{2\mu\rho^2}\left[\frac{1}{\sin 4\vartheta}\frac{\mathrm{d}}{\mathrm{d}\vartheta}\sin 4\vartheta\frac{\mathrm{d}}{\mathrm{d}\vartheta}-\frac{2[J(J+1)-k^2]}{\sin^2 2\vartheta}+n^J_{kvm}\right]\right\}_{\vartheta\to 0} f^J_{kvm}(\vartheta)=0. \quad (35)$$

Equation (35) has solutions

$$f^J_{kvm}(\vartheta)\sim\sin^q 2\vartheta\, P_m^{(0,q)}(\cos 4\vartheta) \quad \text{as} \quad \vartheta\to 0, \quad (36)$$

where the index q is given as

$$q=\{\tfrac{1}{2}[J(J+1)-k^2]\}^{1/2}. \quad (37)$$

The corresponding eigenvalues are given by $n^J_{kvm}=16(m+\frac{1}{2}q)(m+1+\frac{1}{2}q)$.

Combining the asymptotic forms of $f(\vartheta)$, valid at $\vartheta=\frac{1}{4}\pi$ and 0, the solution of (31) may be written as

$$f^J_{kvm}(\vartheta)=\cos^p 2\vartheta\sin^q 2\vartheta\, g^J_{kvm}(\vartheta), \quad (38)$$

where g^J_{kvm} is a well-behaved function of ϑ. In the limit of large ξ, with the substitution of (38), (31) becomes analytically soluble, and the normalised ϑ portion of the unsymmetrised basis function $Y(\Omega)$ is given by

$$f^J_{kvm}(\vartheta)=4\xi^{(p+1)/2}\left[\frac{\Gamma(m+1)}{\Gamma(m+p+1)}\right]^{1/2}\cos^p 2\vartheta\sin^q 2\vartheta$$
$$\times\exp(-\tfrac{1}{2}\xi\cos^2 2\vartheta)\,L_m^p(\xi\cos^2 2\vartheta), \quad (39)$$

where L_m^p is an associated Laguerre polynomial [29] of degree m. In figure 2 the angular form of this function is sketched for low polynomial degrees. In the limit

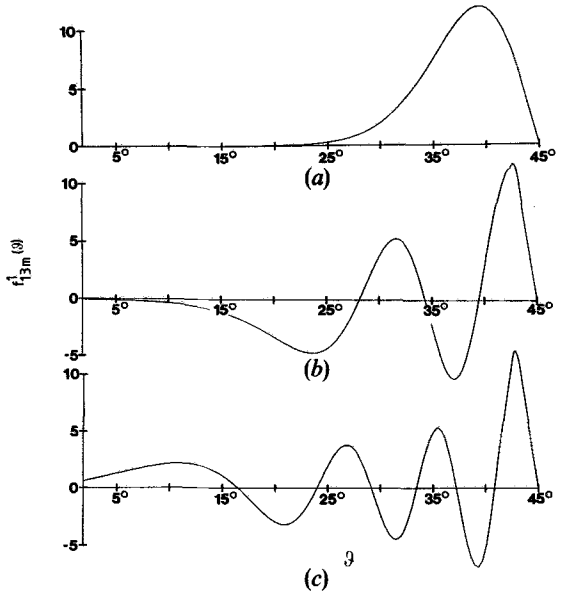

Figure 2. Angular dependence of the basis functions $f^J_{kvm}(\vartheta)$ for $m = 0$ (*a*), 3 (*b*) and 5 (*c*). The functions correspond to the state $J = 1$, $k = 1$ and $v = 3$, with $\xi = 25$.

$\xi \to \infty$ the functions $f(\vartheta)$ form an orthonormal set in ϑ with respect to the volume element $\frac{1}{8}\sin 4\vartheta$. The energy spectrum of the reference Hamiltonian H_0 is equispaced, with eigenvalues

$$E^J_{kvm}(\rho) = \frac{\hbar^2}{2\mu\rho^2}(\Lambda + \tfrac{15}{4} - 8\xi(p+1)) + \frac{4\hbar^2}{\mu\rho^2}\xi m. \tag{40}$$

The normalised angular basis functions $Y(\Omega)$ given by (30) and (39) may be symmetrised by standard techniques [30]. Specifically, for each irreducible representation Γ, we construct the projection operator

$$\hat{\Omega}^\Gamma = \sum_{\mathbf{R}} \omega_\Gamma(\mathbf{R})\hat{\mathbf{R}} \tag{41}$$

where $\hat{\mathbf{R}}$ is one of the symmetry operators of D_{3h}, $\omega_\Gamma(\mathbf{R})$ is the character of $\mathbf{R}$ in Γ and the sum extends over all symmetry operators of D_{3h}. By applying the projection operator $\hat{\Omega}^\Gamma$, for each irreducible representation Γ of D_{3h}, to the unsymmetrised basis function $Y(\Omega)$, we generate the symmetry-adapted basis function $\hat{Y}(\Omega)$ given in (21) together with the symmetry properties summarized in table 1.

The symmetrised basis functions $\hat{Y}(\Omega)$ constitute nearly ideal functions for the expansion of the surface functions Φ. They are orthogonal and complete (in the limit of an infinite set and $\xi \to \infty$). All matrix elements between these functions are finite at the equilateral geometry ($\vartheta = \frac{1}{4}\pi$), and they have simple symmetry properties. However, there are several difficulties, some of which are easily overcome, in using these functions. First, for finite values of ξ the set of symmetrised basis functions $\hat{Y}(\Omega)$ is not strictly orthonormal, although, as we shall show in section 5, the appropriate overlap integrals may be simply evaluated. Secondly, the basis functions do not have the correct limiting behaviour near $\vartheta = 0$, which may lead to unpredictable errors if there is a significant wavefunction amplitude at this point. This problem arises because the basis functions are symmetric-top eigenfunctions with a defined

angular-momentum component along the BF z axis. At $\vartheta = 0$ the Eckart singularity in the principal-axis Hamiltonian (12) requires a coupling of all possible components of the angular momentum along the BF z axis. Any basis function with a defined value of k will have the incorrect asymptotic behaviour at $\vartheta = 0$. However, the basis functions defined above decay sufficiently fast for small ϑ to ensure that all matrix elements remain finite. This has the advantage of ensuring numerical stability, although for potentials with a significant wavefunction amplitude at $\vartheta = 0$ converged eigenvalues are difficult to achieve.

5. Adiabatic surface functions: matrix elements

The surface functions Φ are adiabatic; that is, they depend parametrically upon ρ. Thus, when the surface functions are expanded in terms of the symmetrised basis functions $\hat{Y}(\Omega)$, the coefficients c are functions of ρ (see (19) and (20)). Substitution of the wavefunction expansion (20) into the Schrödinger equation gives the standard matrix equations for the coefficients c in the form

$$\sum_{k'v'm'} (\langle \hat{Y}^{JM\Gamma}_{kvm} | H_a | \hat{Y}^{JM\Gamma}_{k'v'm'} \rangle - U^{J\Gamma}_t(\rho) \langle \hat{Y}^{JM\Gamma}_{kvm} | \hat{Y}^{JM\Gamma}_{k'v'm'} \rangle) c^{J\Gamma t}_{k'v'm'}(\rho) = 0, \tag{42}$$

where, with terms defined as in (12),

$$H_a = T_a + T_r + T_c + \frac{15\hbar^2}{8\mu\rho^2} + V(\rho, \vartheta, \varphi). \tag{43}$$

The matrix elements of the Hamiltonian H_a are described below according to their origin.

The matrix elements of the angular kinetic energy T_a, the Coriolis terms T_c and the symmetric-top part of T_r are obtained from (21), using the properties of Laguerre polynomials, as

$$\begin{aligned}
&\langle \hat{Y}^{JM\Gamma}_{kvm} | T_a + T_{sym} + T_c | \hat{Y}^{JM\Gamma}_{k'v'm'} \rangle \\
&\quad = \frac{\hbar^2}{2\mu\rho^2} \delta_{kk'} \delta_{vv'} \Big\{ 4[(m'+1)(m'+2)(m'+2+p)(m'+1+p)]^{1/2} S_{m,m'+2} \\
&\qquad + 4(2q+\xi)[(m'+1)(m'+1+p)]^{1/2} S_{m,m'+1} \\
&\qquad + 4[q^2 - 2m'(m'+p) + (\xi-1)(2m'+p+1) - 1] S_{m,m'} \\
&\qquad + 4(\xi - 2q)[m'(m'+p)]^{1/2} S_{m,m'-1} \\
&\qquad + 4[m'(m'-1)(m'+p)(m'+p-1)]^{1/2} S_{m,m'-2} \\
&\qquad + 2kv \langle f^J_{kvm} | \frac{1 - \sin 2\vartheta}{\cos^2 2\vartheta} | f^J_{kvm'} \rangle \Big\},
\end{aligned} \tag{44}$$

here the ϑ-overlap integrals $S_{mm'}$ are given by $\langle f^J_{kvm} | f^J_{kvm'} \rangle$, and the indices p and q are defined following (33) and (37). With the substitution $x = \xi \cos^2 2\vartheta$, the overlap integrals $S_{mm'}$ may be written in the form

$$S_{mm'} = 16\xi \left[\frac{\Gamma(m+1)\Gamma(m'+1)}{\Gamma(m+p+1)\Gamma(m'+p+1)} \right]^{1/2} \int_0^\xi x^p \left(1 - \frac{x}{\xi}\right)^q e^{-x} L^p_m(x) L^p_{m'}(x)\, dx. \tag{45}$$

For large values of ξ, corresponding to a deep minimum at $\vartheta = \frac{1}{4}\pi$ in the reference potential $V_0(\rho, \vartheta)$ of (27), the upper limit of the integral may be replaced by infinity without appreciable error. In this case expansion of the term $(1 - x/\xi)^q$ in powers of

x and the use of the result derived by Tennyson and Sutcliffe [4] of

$$I^r_{mm'} = \int_0^\infty e^{-x} x^{p+r} L^p_{m'}(x) L^p_m(x)\, dx$$
$$= (-1)^{m+m'} \sum_{j=0}^{m} \binom{r}{\tau + j}\binom{r}{j} \frac{\Gamma(m + p + r - j + 1)}{\Gamma(m - j + 1)}, \tag{46}$$

where m is chosen so that $\tau = m' - m$ is positive, gives $S_{mm'}$ in terms of the rapidly convergent series

$$S_{mm'} = 16\xi \left[\frac{\Gamma(m+1)\Gamma(m'+1)}{\Gamma(m+p+1)\Gamma(m'+p+1)}\right]^{1/2} \sum_{r=0} \frac{(-1)^r}{\xi^r}\binom{q}{r} I^r_{m'm}. \tag{47}$$

With a similar simplification, the last term within the braces in (44) may be written as

$$2kv\langle f^J_{kvm} | \frac{1 - \sin 2\vartheta}{\cos^2 2\vartheta} | f^J_{kvm'}\rangle = 32kv\xi^2 \left[\frac{\Gamma(m+1)\Gamma(m'+1)}{\Gamma(m+p+1)\Gamma(m'+p+1)}\right]^{1/2}$$
$$\times \int_0^\infty x^{p-1} \left[\left(\frac{1-x}{\xi}\right)^q - \left(\frac{1-x}{\xi}\right)^{q+1/2}\right] e^{-x} L^p_m L^p_{m'}\, dx. \tag{48}$$

This transformed integral may be evaluated efficiently by n-point Gauss–Laguerre quadrature based on the zeros of the polynomial $L^p_n(x)$.

The asymmetric-rotor kinetic energy T_{asy} has matrix elements in the symmetrised basis set that we may write as

$$\langle \hat{Y}^{JM\Gamma}_{kvm} | T_{asy} | \hat{Y}^{JM\Gamma}_{k'v'm'}\rangle = \frac{\hbar^2}{2\mu\rho^2} \langle \hat{Y}^{JM\Gamma}_{kvm} | \frac{\cos 2\vartheta}{\sin^2 2\vartheta} (J_+^2 + J_-^2) | \hat{Y}^{JM\Gamma}_{k'v'm'}\rangle, \tag{49}$$

where the BF angular-momentum raising and lowering operators have been defined according to the identity

$$J_\pm = J_x \mp J_y. \tag{50}$$

The change in sign ensures that the BF angular-momentum operators satisfy commutation relations with the opposite signs to those of the SF operators. With the matrix elements of the raising and lowering operators given by

$$\langle D^{J*}_{Mk} | J_\pm | D^J_{Mk\mp 1}\rangle = \lambda_\pm(J, k), \tag{51}$$

where $\lambda_\pm(J, k) = [(J \pm k + 1)(J \mp k)]^{1/2}$, one readily finds the asymmetric-top terms of (42) may be written as

$$\langle \hat{Y}^{JM\Gamma}_{kvm} | T_{asy} | \hat{Y}^{JM\Gamma}_{k'v'm'}\rangle = \frac{\hbar^2}{2\mu\rho^2} \langle f^J_{kvm} | \frac{\cos 2\vartheta}{\sin^2 2\vartheta} | f^J_{k'v'm'}\rangle$$
$$\times \{[1 + (-1)^{J+k+\sigma}\delta_{k0}\,\delta_{v0}][1 + (-1)^{J+k'+\sigma}\delta_{k'0}\,\delta_{v'0}]\}^{1/2}$$
$$\times [\lambda_+(J, k)\lambda_+(J, k+1)\delta_{k', k'+2}\,\delta_{v, v'}$$
$$+ \lambda_-(J, k)\lambda_-(J, k-1)\delta_{k', k-2}\,\delta_{v, v'}$$
$$+ (-1)^{J+k+\sigma}\lambda_-(J, k)\lambda_-(J, k-1)\delta_{k', 2-k}\,\delta_{v, -v'}], \tag{52}$$

where the symmetry properties require that we need only consider elements with k and $k' \geqslant 0$. We note that the last term in the final set of square brackets in (52) is zero for all states with k or $k' \geqslant 2$. The ϑ integral may be evaluated using the same Gaussian methods as for the kinetic-energy terms above. Substitution of the asymptotic small-ϑ form for the function f, (36), demonstrates that the asymmetric-rotor terms remain finite near $\vartheta = 0$.

The angular potential $V(\rho, \vartheta, \varphi)$, with ρ fixed, is invariant under all the symmetry operations of D_{3h}. The potential may be expanded in the Fourier series

$$V(\rho, \vartheta, \varphi) = 2 \sum_n \bar{V}_{6n}(\vartheta; \rho) \cos 6n\varphi, \tag{53}$$

where $\bar{V}_{6n}$ is a Fourier coefficient that depends parametrically upon ρ. With this expansion, the potential-matrix elements simplify to

$$\begin{aligned}
&\langle \hat{Y}^{JM\Gamma}_{kvm} | V(\rho, \vartheta, \varphi) + \frac{15\hbar^2}{2\mu\rho^2} | \hat{Y}^{JM\Gamma}_{k'v'm'} \rangle \\
&= \frac{15\hbar^2}{2\mu\rho^2} \delta_{kk'} \delta_{vv'} \delta_{mm'} + \{[1 + (-1)^{J+k+\sigma}\delta_{k0}\delta_{v0}][1 + (-1)^{J+k'+\sigma}\delta_{k'0}\delta_{v'0}]\}^{1/2} \\
&\quad \times \sum_n \langle f^J_{kvm} | \bar{V}_{6n} | f^J_{k'v'm'} \rangle (1 + \delta_{n0})[\delta_{6n, v'-v} + (-1)^{J+k+\sigma}\delta_{6n, v'-v}\delta_{k,0}]
\end{aligned} \tag{54}$$

The integrals are evaluated using the quadrature methods described above, while the Fourier coefficients $\bar{V}_{6n}$ are rapidly determined using fast-Fourier-transform methods.

6. The radial wavefunction: inclusion of non-adiabaticity

The adiabatic surface function Φ depends parametrically upon ρ. Thus, when the expansion of (18) is substituted into the full Schrödinger equation (10), the resulting coupled-channel equations for the radial wavefunction χ are of the form

$$\left\{\frac{d^2}{d\rho^2} + \frac{2\mu}{\hbar^2}[E - U^{J\Gamma}_t(\rho)]\right\}\chi^{J\Gamma}_t(\rho) = \sum_{t'}^{N_{t'}} \left[Y^{J\Gamma}_{tt'}(\rho) + X^{J\Gamma}_{tt'}(\rho) \frac{d}{d\rho} \right] \chi^{J\Gamma}_{t'}(\rho), \tag{55}$$

where the non-adiabatic matrix elements $X(\rho)$ and $Y(\rho)$ are defined as

$$\left.\begin{aligned}
X^{J\Gamma}_{tt'}(\rho) &= \langle \Phi^{JM\Gamma}_t(\Omega; \rho) | -2 \frac{\partial}{\partial\rho} | \Phi^{JM\Gamma}_{t'}(\Omega; \rho) \rangle, \\
Y^{J\Gamma}_{tt'}(\rho) &= \langle \Phi^{JM\Gamma}_t(\Omega; \rho) | -\frac{\partial^2}{\partial\rho^2} | \Phi^{JM\Gamma}_{t'}(\Omega; \rho) \rangle,
\end{aligned}\right\} \tag{56}$$

with the integration restricted to the set of angular coordinates Ω. We seek a solution to this set of coupled equations by assuming that motion in the radial coordinate ρ is 'locally separable' from motion in the angular coordinates Ω. Corrections to this adiabatic assumption will be included by perturbation theory. The coupled equations (55) are formally identical with the equations for nuclear motion in a diatomic molecule within the Born–Oppenheimer approximation, if ρ is identified with the internuclear distance and Ω refers to the electronic coordinates. The smallness of the non-adiabatic coupling terms arise in this case because of the

difference in the characteristic frequencies of electronic and nuclear motion. The equations for the nuclear motion, analogous to (55), are only weakly coupled, so accurate solutions may be calculated with a perturbative treatment of the non-adiabatic terms. However, an adiabatic-type separation is also valid if angular and radial motions are of comparable frequencies, provided that the angular wavefunction Φ depends only slowly upon the radial coordinate. A weak radial dependence of Φ arises if the ratio of the angular kinetic energy to the angular potential energy in (19) varies smoothly with the radial coordinate ρ. Significant non-adiabatic coupling terms are expected in regions of ρ where, for example, the minimum of the angular potential shifts with ρ.

In the isotropic limit of no coupling ($V(\rho, \vartheta, \varphi) \rightarrow V(\rho)$) the non-adiabatic coupling terms in (55) must vanish, and the coupled radial equations reduce to the set of one-dimensional equations

$$\left\{\frac{d^2}{d\rho^2} + \frac{2\mu}{\hbar^2}[E^0 - U_t^{J\Gamma}(\rho)]\right\}{}^{(0)}\chi_t^{J\Gamma}(\rho) = 0, \tag{57}$$

where ${}^{(0)}\chi$ may be taken as a zeroth-order approximation to the radial wavefunction χ in (18) and E^0 is the corresponding zeroth-order eigenvalue. The radial Schrödinger equation (57) can be solved using a variety of methods. We have used the Numerov–Cooley finite-element algorithm [31], which is both efficient and accurate. By analogy with the electronic Born–Oppenheimer approximation, it can easily be shown [32] that the zeroth-order energy E^0 is necessarily a lower bound to the exact energy of the ground state. If, however, the diagonal coupling term $Y_{tt}(\rho)$ is included in (57),

$$\left\{\frac{d^2}{d\rho^2} + \frac{2\mu}{\hbar^2}[E^1 - U_t^{J\Gamma}(\rho)] - Y_{tt}^{J\Gamma}(\rho)\right\}{}^{(1)}\chi_t^{J\Gamma}(\rho) = 0, \tag{58}$$

then the resulting energy E^1, which includes terms up to first order in the non-adiabatic coupling, is just the expectation value of the full Hamiltonian for the approximate 'locally separable' wavefunction of the form

$${}^{(1)}\psi_t^{JM\Gamma} = {}^{(1)}\chi_t^{J\Gamma}(\rho)\Phi_t^{JM\Gamma}(\Omega; \rho). \tag{59}$$

From the variational principle, E^1 is rigorously an upper bound to the exact energy of the ground state. The energy of the ground state is therefore bounded by the values E^0 and E^1.

The exact solution to the set of weakly coupled differential equations (55) may be found by perturbation theory. We have used an iterative Brillouin–Wigner procedure, which has the advantage that, compared with the conventional Rayleigh–Schrödinger treatment, the effects of higher-order terms may readily be included. The numerical implementation of this procedure has been described in detail elsewhere [21].

Corrections to the 'locally separable' zeroth-order wavefunction require the computation of integrals of the radial derivatives of the angular wavefunction Φ. These non-adiabatic terms may be evaluated either in terms of matrix elements of the derivative of the potential [33] or via a finite-difference approach [34]. Here we use the latter method for reasons of computational ease. If the angular surface function $\Phi(\Omega; \rho)$ is evaluated at the N equally spaced radial grid points $\rho_k = \rho_0 + k\,\Delta\rho$ ($k = 0, \ldots, N-1$) then the derivative at $\rho = \rho_{k+1/2}$ may be approximated

by the central-difference result

$$\left[\frac{\partial \Phi_t^{JM\Gamma}(\Omega;\rho)}{\partial \rho}\right]_{\rho=\rho_{k+1/2}} = \frac{1}{\Delta\rho}\left[\Phi_t^{JM\Gamma}(\Omega;\rho_{k+1}) - \Phi_t^{JM\Gamma}(\Omega;\rho_k)\right]. \tag{60}$$

Substituting this result into (56) gives the non-adiabatic matrix elements in terms of the overlap of the angular surface function at neighbouring points of the ρ grid:

$$X_{tt'}^{J\Gamma}(\rho_{k+1/2}) = \frac{1}{\Delta\rho}\left[T_{t't}^{J\Gamma}(\rho_k) - T_{tt'}^{J\Gamma}(\rho_k)\right]$$

$$Y_{tt'}^{J\Gamma}(\rho_{k+1/2}) = \frac{1}{\Delta\rho^2}\left[2\delta_{tt'} - T_{tt'}^{J\Gamma}(\rho_k) - T_{t't}^{J\Gamma}(\rho_k)\right] + \frac{1}{2}\frac{\mathrm{d}}{\mathrm{d}\rho}X_{tt'}^{J\Gamma}(\rho_{k+1/2}), \tag{61}$$

where the transfer-matrix element $T(\rho_k)$ is defined in terms of the Ω integral:

$$T_{tt'}^{J\Gamma}(\rho_k) = \langle \Phi_t^{J\Gamma}(\Omega;\rho_k) | \Phi_{t'}^{J\Gamma}(\Omega;\rho_{k+1})\rangle. \tag{62}$$

This integral may be calculated efficiently using the quadrature techniques discussed in section 5.

7. Results for H_3^+

7.1. *Potential-energy surfaces*

Calculations were performed for the configuration-interaction surface of Carney and Porter (CP) [13] and the variationally superior surface of Schinke, Dupuis and Lester (SDL) [12]. The fitting procedure used by Schinke *et al.* does not, however, ensure that the potential function is totally symmetric. In our calculations the potential was symmetrised by the following device. At each value of $(\rho, \vartheta, \varphi)$ the three equivalent sets of Jacobi coordinates were calculated. The potential was evaluated for the coordinate set that maximised the ratio of the proton–H_2 distance to the diatomic H_2 internuclear separation, thus ensuring that symmetric geometries were always treated equivalently.

7.2. *Vibrational-basis-set selection and convergence checks*

As a first step towards the accurate calculation of the vibrational eigenvalues of H_3^+, the calculational methods described in sections 5 and 6 were optimised. In the adiabatic hyperspherical technique there are at least three parameters that can be varied: the constant ξ in the angular basis function $\hat{Y}(\Omega)$, which determines the rate of decay of the angular amplitude as $\vartheta \to 0$; the size of the angular basis set used to represent the adiabatic surface function $\Phi(\Omega;\rho)$, and the number of radial channels $N_{t'}$ included in the iterative Brillouin–Wigner solution of the coupled radial equations (55). The optimum values of these parameters were found by studying the convergence of the final energies. Since the form of the angular basis set is different for each of the three vibrational symmetries, separate convergence studies were required for each symmetry species. However, apart from the number and symmetry of the angular basis functions, the optimum values of the other parameters were found to be very similar for all symmetries. We shall therefore confine our dis-

cussion to the convergence of the vibrational states of A_1' symmetry on the CP surface.

We start by optimising the value of ξ. At each value of ρ, ξ was chosen to minimise the lowest eigenvalue of the angular Hamiltonian (43). For the Carney and Porter surface, ξ was determined as

$$\xi = \begin{cases} 30{\cdot}0 & (0{\cdot}54\,\text{Å} \leqslant \rho \leqslant 0{\cdot}90\,\text{Å}), \\ 25{\cdot}0 & (0{\cdot}90\,\text{Å} < \rho \leqslant 2{\cdot}06\,\text{Å}). \end{cases} \tag{63}$$

The effect on the A_1' eigenvalues of a small variation in the parameter ξ from its optimum value is shown in table 2. The angular kinetic and potential matrix elements were evaluated using a 30-point Gaussian-quadrature rule. The Fourier coefficients $\bar{V}_{6n}(\vartheta; \rho)$ were calculated using a 64-point fast Fourier transform of the potential $V(\rho, \vartheta, \varphi)$.

Once the optimum value of ξ had been determined, the number of angular basis functions $\hat{Y}(\Omega)$ to be included in the matrix diagonalisation of the angular Hamiltonian H_a was found in a series of trial conditions. For each symmetry species the adiabatic surface function $\Phi(\Omega; \rho)$ was expanded in the set of angular basis functions $\hat{Y}_{kvm}(\Omega)$, where for the vibrational states $k = 0$. The values of the kinematic quantum number v in this sum are determined by the state symmetry and are listed in table 1 as the set $\pm[v]$. The angular basis functions $\hat{Y}_{0vm}$ and $\hat{Y}_{0-vm}$ are identical apart from a phase factor (see (21)). Hence for states of $k = 0$ the kinematic quantum number v can be further restricted to the set $[v]$. In table 3 the optimised angular basis sets are listed for the three vibrational symmetries. Convergence checks, detailed in table 4,

Table 2. Convergence of A_1' ($J = 0$) eigenvalues† with respect to ξ‡.

Vibrational state (v_1, v_2, l_2)	$\xi = \xi^*$§	$\xi = \xi^* + 2{\cdot}5$§
(0, 0, 0)	4345·106	4345·106
(1, 0, 0)	7529·849	7529·849
(0, 2, 0)	9133·160	9133·171
(2, 0, 0)	10603·975	10603·974
(0, 3, 3)	11668·64	11669·14
(1, 2, 0)	12115·30	12115·34

† Eigenvalues in cm^{-1} for CP surface relative to potential minimum.
‡ Angular basis set described in table 3, 10 non-adiabatic channels.
§ ξ^* is given by (63).

Table 3. The angular basis functions used in vibrational calculations.

Vibrational-state symmetry	(v_{min}, v_{max})†	n_{max}‡	Basis size
A_1'	(0, 18)	6	28
A_2'	(6, 24)	6	28
E′	(−20, 16)	6	49

† The quantum number v lies in the range $v_{min} \leqslant v \leqslant v_{max}$.
‡ Maximum degree of Laguerre polynomial.

Table 4. Convergence of A_1' ($J = 0$) eigenvalues† with respect to angular basis size‡.

Vibrational state (v_1, v_2, l_2)	m_{max}, v_{max}§ (6, 12)	(5, 18)	(6, 18)
(0, 0, 0)	4345·107	4345·107	4345·106
(1, 0, 0)	7529·853	7529·851	7529·849
(0, 2, 0)	9133·788	9133·217	9133·160
(2, 0, 0)	10603·984	10603·975	10603·976
(0, 3, 3)	11676·13	11671·77	11668·64
(1, 2, 0)	12116·30	12115·52	12115·30

† Eigenvalues in cm^{-1} for the CP surface.

‡ ξ fixed at values given by (63), 10 non-adiabatic channels.

§ Maximum degree of Laguerre polynomial and maximum value of v included in the angular basis set. The basis set includes all states $0 \leqslant v \leqslant v_{max}$.

show that the low-lying states are very closely converged ($<0{\cdot}01\ cm^{-1}$), with higher eigenvalues being converged to better than $1\ cm^{-1}$.

In the final step of the calculation the non-adiabatic correction terms were included via Brillouin–Wigner perturbation theory. The angular Hamiltonian was diagonalised for 77 equally spaced values of the radial coordinate ρ in the range $0{\cdot}54\ Å \leqslant \rho \leqslant 2{\cdot}06\ Å$. Figure 3 depicts the radial dependence of the eigenvalues $U(\rho)$ of the angular Hamiltonian for solutions of A_1' symmetry. To achieve energies accurate to $0{\cdot}01\ cm^{-1}$, the eigenvalues $U(\rho)$ and the non-adiabatic matrix elements $X(\rho)$ and $Y(\rho)$ were interpolated, using the method of cubic splines, onto an equally spaced fine grid of 751 points. To complete the calculation and converge the pertur-

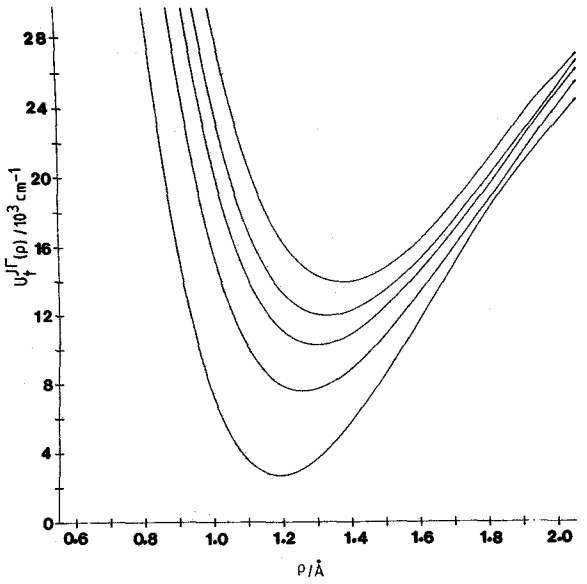

Figure 3. Radial dependence of the eigenvalues $U_i^{J\Gamma}(\rho)$ of the fixed-ρ angular Hamiltonian for the vibrational states ($J = 0$) of A_1' symmetry. Calculations are for the surface of Carney and Porter.

Table 5. Convergence of A_1' ($J = 0$) eigenvalues† with respect to number of non-adiabatic channels included in iterative Brillouin–Wigner solution‡.

Vibrational state (v_1, v_2, l_2)	N_t§		Rayleigh–Schrödinger‖		
	6	10	E^0	E^1	E^2
(0, 0, 0)	4345.106	4345·106	4341·156	4347·503	4345·113
(1, 0, 0)	7529·849	7529·849	7536·185	7545·840	7529·769
(0, 2, 0)	9133·176	9133·160	9109·439	9148·759	9133·512
(2, 0, 0)	10603·976	10603·975	10613·445	10632·280	10603·538
(0, 3, 3)	11669·19	11668·64	11735·43	11811·08	11644·08
(1, 2, 0)	12115·62	12115·30	12026·93	12100·98	12131·96

† Eigenvalues in cm^{-1} for CP surface.

‡ Calculation with ξ fixed at values given by (63), and the angular basis described in table 3.

§ Number of non-adiabatic channels included in iterative Brillouin–Wigner solution.

‖ Results of zeroth-, first- and second-order Rayleigh–Schrödinger perturbation theory.

bation solution of the coupled radial equations, an iterative form of Brillouin–Wigner perturbation theory was used. Table 5 illustrates the rapid convergence of the perturbation calculation with the number of radial channels N_t, included in the iterative solution. Ten radial channels ensure convergence to within $0{\cdot}01\,cm^{-1}$. The zeroth-, first- and second-order Rayleigh–Schrödinger energies are also given for comparison.

The zeroth- and first-order energies, as discussed in section 6, bracket the exact ground-state energy. The small shift of about $4\,cm^{-1}$ between the zeroth-order and exact energies shows that the assumption of an adiabatic separation between radial and angular motion is justified. Table 5 shows that the non-adiabatic correction terms become increasingly significant as the vibrational energy increases. The reasons for this are illustrated in figure 4, where the non-adiabatic matrix elements between the ground and first excited A_1' channels are plotted as a function of ρ. The non-adiabatic matrix elements show a sharp peak at $\rho \approx 1{\cdot}8$ Å, where the character of the angular eigenfunctions changes rapidly. Stereographic projections of the potential, similar to figures 1(*b*) and (*c*), show that at this value of ρ the angular minimum shifts from the equilateral geometry towards a near-collinear geometry. The high-energy vibrational states sample this large-ρ portion of the potential-energy surface, and hence the non-adiabatic correction terms become more significant.

7.3. *Rotational-basis-set selection*

In H_3^+ the body-fixed z projection k of the total angular momentum is not strictly a conserved quantity. Thus at each J and Γ the matrix representation of the angular Hamiltonian has a blocked structure with submatrices $(J\Gamma\,|\,k\,|)$, diagonal in the BF projection quantum number $|k|$, coupled by asymmetric-top matrix elements that are off-diagonal in $|k|$. Each submatrix $(J\Gamma\,|\,k\,|)$ is composed of matrix elements of the angular Hamiltonian in the set of symmetrised angular basis functions $\hat{Y}_{|k|vm}(\Omega)$ with k fixed and the kinematic quantum number v limited to the symmetry sets $\pm[v]$ listed in table 1. The functions $\hat{Y}_{|k|vm}$ and $\hat{Y}_{|k|-vm}$ are inequivalent, apart from the special case of $k = 0$, where they differ by a trivial phase factor.

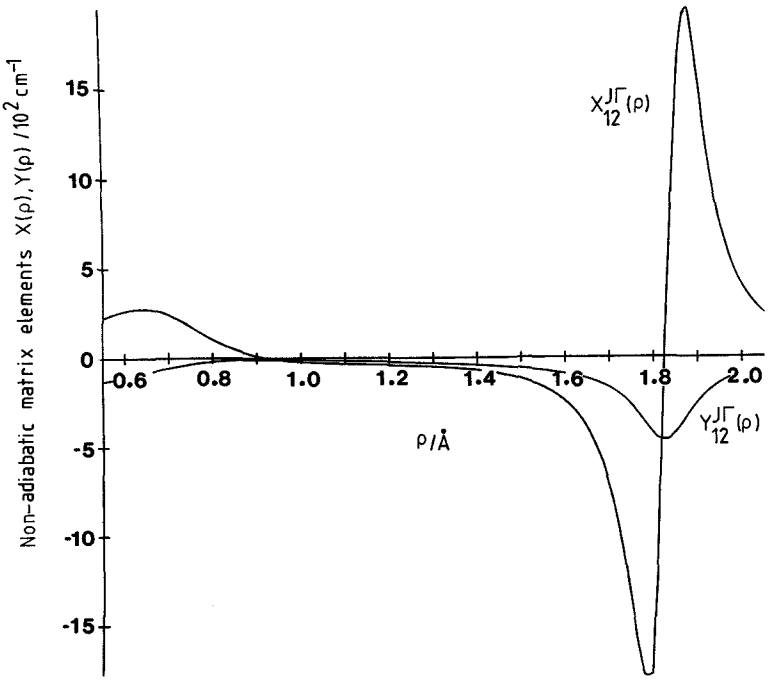

Figure 4. Radial dependence of the non-adiabatic matrix elements $X_{12}^{J\Gamma}(\rho)$ and $Y_{12}^{J\Gamma}(\rho)$ for $J = 0$ and symmetry $\Gamma = A_1'$, between the ground-state adiabatic surface function $\Phi_1^{JM\Gamma}(\Omega; \rho)$ and the first excited state $\Phi_2^{JM\Gamma}(\Omega; \rho)$. Calculations are for the surface of Carney and Porter.

For a complete rovibrational calculation both functions must be included in the matrix representation $(J\Gamma \mid k \mid)$ for non-zero k.

For states of E symmetry the size of the angular basis set may be reduced by the use of an approximate symmetry classification. Equations (44), (52) and (54) demonstrate that the matrix elements of the angular Hamiltonian obey the selection rule $\Delta v = 0 \pmod 6$, with the single exception of the asymmetric-top kinetic-energy operator, which connects the functions $\hat{Y}_{|k|vm}$ and $\hat{Y}_{|k'|-vm}$ if k and $k' \leqslant 2$. In states of A_1 and A_2 symmetry v is a multiple of three, so matrix elements between $\hat{Y}_{|k|vm}$ and $\hat{Y}_{|k'|-vm}$ satisfy the selection rule $\Delta v = 0 \pmod 6$ and are generally non-zero. However, for states of E symmetry, where v is not a multiple of three, only asymmetric-top terms connect these two functions. In the conventional normal-mode description of H_3^+ [35] the two angular basis functions $\hat{Y}_{|k|vm}$ and $\hat{Y}_{|k|-vm}$ correspond to rotational levels of different vibrational l_2 manifolds, where l_2 is the vibrational angular momentum quantum number associated with the degenerate bending mode ν_2. Perturbation arguments suggest that the effect of these vibrational off-diagonal terms will be small consequently we shall ignore them here. With neglect of these terms, the submatrix $(J\Gamma \mid k \mid)$ may be partitioned into two, with the kinematic quantum number v limited to the set $+[v]$ in the upper partition and to $-[v]$ in the lower partition.

For the general rovibrational problem the optimum size of the angular basis is found by methods similar to those described in section 7.2. Table 6 lists the angular basis sets used in the rotational calculations of H_3^+ described below. All other

Table 6. Angular basis functions used in the rovibrational calculations.

Irreducible representation	(v_{min}, v_{max})†	
	$k = 0$	$k \neq 0$
A_1'	(0, 18)	(−18, 18)
A_1''	—‡	(−21, 21)
A_2'	(6, 24)	(−18, 18)
A_2''	—‡	(−21, 21)
E′(+)§	(−16, 20)	(−16, 20)
E′(−)§	(−20, 16)	(−20, 16)
E″(+)§	—‡	(−17, 19)
E″(−)§	—‡	(−19, 17)

† Minimum and maximum values of the kinematic quantum number v. Laguerre polynomials of maximum degree six were used in all rotational calculations.

‡ Symmetry-forbidden.

§ +/− labels the E states by the approximate symmetry classification described in the text.

parameters were constrained at the optimum values found in the purely vibrational calculations described in section 7.2.

7.4. *Vibrational and rotational results*

The vibrational states of H_3^+ are conventionally labelled by the quantum numbers $(v_1, v_2, |l_2|)$ where v_1 refers to the totally symmetric (A_1') vibrational mode and v_2 to the doubly degenerate (E′) bending vibration. In states where the degenerate vibration is excited, H_3^+ has a vibrational angular momentum about the symmetry axis that takes values of $l_2 = -v_2, -v_2 + 2, \ldots, v_2 - 2, v_2$. The D_{3h} symmetry of the vibrational state $(v_1, v_2, |l_2|)$ is determined by l_2. States of $l_2 = \pm 3, \pm 6, \ldots$, correspond to A_1', A_2' pairs, $l_2 = 0$ transform as A_1', while all other values of l_2 belong to E′ symmetry representations. For H_3^+ the nuclear-spin statistics imply that only rotational–vibrational levels of overall symmetry A_2 or E are populated. Levels of symmetry A_1' and A_1'' have zero statistical weight.

Table 7 gives our results for the $J = 0$ states of H_3^+ of each symmetry species on the potential-energy surfaces of Carney and Porter (CP) and Schinke, Dupuis and Lester (SDL). The vibrational states of A_1' symmetry are not populated, but we present them for completeness. We also give the results of the calculation of Carney and Porter [13] (using a Watson Hamiltonian) for the CP surface and Tennyson and Sutcliffe [6] (using Jacobi coordinates) for the SDL surface. While minor differences exist between the present calculations for the SDL surface and those reported by Tennyson and Sutcliffe (the E′ calculated modes being averaged when perfect degeneracy is not achieved), the overall agreement is very good. Our results for the CP surface, however, are consistently lower than those obtained by Carney and Porter for the same surface. Since we have demonstrated that the low-lying vibrational band origins are converged to 0·01 cm^{-1} or better, this disagreement must be due either to a lack of basis-set convergence in the calculations of Carney and Porter or an incomplete treatment of the divergent terms that occur in the Watson Hamiltonian at linear geometries.

Table 7. Vibrational eigenvalues† of H_3^+.

	Vibrational state (v_1, v_2, l_2)	CP surface [13]		SDL surface [12]	
		This work	[13]‡	This work	[6]‡
A_1'	(0, 0, 0)	4345·106	4345·28	4330·472	4330·54§
	(1, 0, 0)	7529·849	7530·49	7521·430	7521·6
	(0, 2, 0)	9133·160	9144·47	9055·299	9055·5
	(2, 0, 0)	10603·975	10613·05	10607·067	10606·8
	(0, 3, 3)	11668·64		11566·45	11565·5
	(1, 2, 0)	12115·30		12069·07	12070·8
A_2'	(0, 3, 3)	11833·800		11781·384	11781·8
	(1, 3, 3)	14576·373		14503·526	
	(0, 5, 3)	15935·02		15800·41	
	(2, 3, 3)	17214·3		17115·9	
	(1, 5, 3)	18245·8		18026·8	
	(0, 6, 6)	19062·2‖			
	(3, 3, 3)	19709·1			
	(2, 5, 3)	20533·9			
E′	(0, 1, 1)	6860·607	6861·36	6824·722	6824·9
	(0, 2, 2)	9340·464	9349·05	9288·58	9288·7
	(1, 1, 1)	9903·916	9913·09	9875·91	9875·6
	(0, 3, 1)	11383·0		11275·06	11274·4
	(1, 2, 2)	12231·8		12177·92	
	(2, 1, 1)	12835·2		12821·71	
	(1, 3, 1)	14350·4			
	(2, 2, 2)	15016·8			

† Eigenvalues in cm^{-1} relative to potential minimum.
‡ Averaged over degnerate pairs.
§ Corrected zero-point energy.
‖ Eigenvalue not completely converged.

Tables 8 and 9 give the predicted rotational levels for the ground state and the first two fundamentals of H_3^+. For comparison, the results of Carney and Porter [17] and Tennyson and Sutcliffe [6] are also presented. The experimental rotational levels of the ground state and $v_2 = 1$ states are determined from the spectroscopically fitted parameters and common differences given by Oka and collabo-

Table 8. Rotational eigenvalues† of ground state and the $v_1 = 1$ vibration of H_3^+.

Rotational state				CP surface [13]			SDL surface [12]		
				Ground state		$v_1 = 1$	Ground state		$v_1 = 1$
J	k	sym	Expt [36]	This work	[17]‡	This work	This work	[6]‡	This work
1	1	E″	64·12	63·75	64·30	62·12	64·05	64·05	62·70
1	0	A_2'	86·96	86·38	87·24	84·28	86·87	86·87	84·90
2	2	E′	169·27	168·18	169·78	163·79		169·08	
2	1	E″	237·35	236·22	238·04	230·38		237·09	
2	0	A_1'		258·18	260·67	251·88	260·24	259·62	254·34

† Eigenvalues in cm^{-1} relative to vibrational origins given in Table 7.
‡ Averaged over degenerate pairs.

Table 9. Rotational eigenvalues† of H_3^+ in $v_2 = 1$ vibration.

Rotational level						CP surface [13]		SDL surface [12]	
J	k	sym	G	U	s	Expt [36]	This work	This work	[6]‡
1	1	E″	2	+1		26·73	26·42	27·07	25·8
1	0	E′	1	+1		88·13	87·62	88·19	87·0
1	1	A_2''	0	−1	+1	95·28	95·18	94·69	93·6
1	1	A_1''	0	+1	−1		105·37	105·94	104·8
2	2	A_1'	3	+1	+1		91·88		92·0
2	2	A_2'	3	+1	−1	92·81	91·88		92·1
2	1	E″	2	+1		202·53	201·36		201·7
2	2	E′	1	−1		234·15	233·69		231·0
2	0	E′	1	+1		268·93	267·24		268·2
2	1	A_1''	0	−1	+1		259·32		257·9
2	1	A_2''	0	+1	−1	291·45	289·38		290·8

† Eigenvalues in cm^{-1} relative to $v_2 = 1$ vibrational origin given in Table 2.
‡ Averaged over degenerate pairs.

rators [36]. The predicted rotational levels of several overtone bands are given in tables 10 and 11. The rotational levels have been labelled by the quantum numbers J and k for non-degenerate vibrations and J and $G = |k - l_2|$ for degenerate vibrations. States of non-zero k/G that are a multiple of three form A_1, A_2 pairs. All other non-zero k/G levels have E symmetry. In the notation introduced by Watson [35] the rotational levels of degenerate vibrations may be further characterised by the value $\pm U$, which distinguishes upper and lower components of the l resonance, and $s = \pm 1$, which differentiates the components of the symmetry pair A_1, A_2 for $G = 0$ (mod 3). The quantum number U is defined so that the equivalent oblate-top quantum number k is given by $k = |G - U|$.

The agreement between the present calculations and those of Tennyson and Sutcliffe is seen as essentially exact for the ground-state rotational levels. However, we note that the present results for the $v_2 = 1$ manifold differ from the calculations of Tennyson and Sutcliffe by over $1\,cm^{-1}$. Since both calculations appear to be converged to better than $0{\cdot}1\,cm^{-1}$, we are uncertain of the origin of this discrepancy. Table 9 does, however, show that the present results for the $v_2 = 1$ state are in closer agreement with the experimental values than those reported by Tennyson and Sutcliffe. The rovibrational levels obtained on the CP surface are consistently lower

Table 10. Rotational eigenvalues† of $v_1 = 2$ and $v_2 = 2$, $l_2 = 0$ vibrational states of H_3^+.

Rotational state			CP surface [13]		SDL surface [12]	
J	k	sym	$v_1 = 2$	$v_2 = 2, l_2 = 0$	$v_1 = 2$	$v_2 = 2, l_2 = 0$
1	1	E″	60·49	64·21		64·99
1	0	A_2'	82·21	91·32	82·89	92·21
2	2	E′	159·35	163·74		
2	1	E″	224·61	246·38		
2	0	A_1'	245·71	269·63	248·38	276·04

† Eigenvalues in cm^{-1} relative to vibrational origins given in Table 7.

Table 11. Rotational eigenvalues† of $v_2 = 2, l_2 = \pm 2$ and $v_1 = 1, v_2 = 1$ vibrations of H_3^+.

	Rotational level							
	J	k	sym	G	U	s	CP surface [13]	SDL surface [12]
$v_2 = 2, l_2 = \pm 2$	1	1	A_2''	3	+2	+1	−4·43	−2·42
	1	1	A_1''	3	+2	−1	−0·95	1·79
	1	0	E′	2	+2		88·99	89·75
	1	1	E″	1	+2		128·23	126·40
	2	2	E′	4	+2		31·59	
	2	1	A_1''	3	+2	+1	169·79	
	2	1	A_2''	3	+2	−1	179·77	
	2	0	E′	2	+2		266·45	
	2	1	E″	1	+2		305·94	
	2	2	A_1'	0	−2	+1	291·18	
	2	2	A_2'	0	+2	−1	291·35	
$v_1 = 1, v_2 = 1$	1	1	E″	2	+1		28·55	30·31
	1	0	E′	1	+1		85·63	86·30
	1	1	A_2''	0	−1	+1	91·03	89·94
	1	1	A_1''	0	+1	−1	100·37	100·00
	2	2	A_1'	3	+1	+1	96·09	
	2	2	A_2'	3	+1	−1	96·23	
	2	1	E″	2	+1		199·42	
	2	2	E′	1	−1		229·77	
	2	0	E′	1	+1		256·26	
	2	1	A_1''	0	−1	+1	252·22	
	2	1	A_2''	0	+1	−1	279·76	

† Eigenvalues in cm^{-1} relative to vibrational origins given in Table 7.

than either the experimental values or those given by the SDL surface. The rotational constants are roughly proportional to the inverse square of the equilibrium internuclear distance, which suggests that the bond length of the CP surface is too high.

For the general rovibrational problem the complete inclusion of the asymmetric-top terms requires an angular basis set that increases in size approximately as $\frac{1}{2}J$. As discussed in section 1, the embedding of the BF axes in the SW hyperspherical coordinate system is expected to minimise these coupling terms for oblate-top molecules such as H_3^+. This suggests that an angular-momentum decoupling scheme may be applicable. The basis of this approximation is the complete neglect in the angular Hamiltonian matrix of all off-diagonal (in $|k|$) asymmetric-top matrix elements. We do, however, retain the diagonal (in $|k|$) asymmetric-top elements for the level $|k| = 1$, i.e. the last term in the final set of brackets in (52). At each J and Γ the angular Hamiltonian is now partitioned into the smaller submatrices $(J\Gamma|k|)$ labelled by the diagonal quantum number $|k|$. In table 12 we list a direct comparison between the exact and decoupled results for H_3^+ $J = 2$ levels of E′ symmetry. These trial calculations suggest that neglect of the Coriolis interactions is a reasonable approximation for most rovibrational levels, with the decoupled energies differing from the exact energies by less than about $2\,cm^{-1}$. Previous calculations [37] have highlighted the failure in H_3^+ of a rotational-decoupling approximation for BF coordinate systems aligned with the z axis in the molecular plane. As pointed out above, this choice results in a maximum coupling of the various BF angular-

Table 12. $J = 2$, E′ rotational levels† of H_3^+ calculated on the CP potential surface. Comparison of the results of fully coupled and decoupled calculations.

Vibration	Rotational level					
(v_1, v_2, l_2)	J	k	G	U	Fully coupled‡	Decoupled§
(0, 0, 0)	2	2	2		4513·289	4513·566
(0, 1, 1)	2	2	1	−1	7094·293	7100·259
(0, 1, 1)	2	0	1	+1	7122·864	7123·022
(1, 0, 0)	2	2	2		7693·634	7693·883
(0, 2, 0)	2	2	2		9296·902	9298·431
(0, 2, 2)	2	2	4	+2	9372·299	9372·026
(0, 2, 2)	2	0	2	+2	9608·712	9606·914
(1, 1, 1)	2	2	1	−1	10129·15	10133·682
(1, 1, 1)	2	0	1	+1	10164·013	10160·370
(2, 0, 0)	2	2	2		10763·325	10763·548

† Eigenvalues in cm^{-1}.
‡ Results for the fully coupled calculations.
§ Results for complete neglect of off-diagonal Coriolis interactions.

momentum components, and the agreement found between exact and decoupled rotational energies is correspondingly poor, with differences of up to about $50\,cm^{-1}$ [37]. Relatively accurate calculations of highly excited rotational states may therefore be feasible in hyperspherical coordinates with the use of a decoupling approximation to reduce the size of the calculation.

8. Summary and concluding remarks

In this paper we have presented a method for performing rovibrational calculations in triatomic molecules with large-amplitude internal motions. Our approach uses an adiabatic separation of radial and angular motions in the symmetric hyperspherical coordinate system introduced by Smith and Whitten [8]. For rovibrational levels of total angular momentum J and symmetry Γ, the eigenfunctions of the angular Hamiltonian are expressed in terms of symmetrised products of angular-momentum eigenfunctions and hyperspherical basis functions. The behaviour of the angular Hamiltonian at those critical configurations where some of the hyperspherical coordinates are undefined fixes the asymptotic form of the hyperspherical basis functions. The radial wavefunction is defined by a set of coupled differential equations, which in the limit of weak coupling may be solved by an iterative form of Brillouin–Wigner perturbation theory [21]. In principle, this method is exact.

We have applied this method to a calculation of the low-lying rovibrational states of H_3^+, a molecule chosen largely because of its large-amplitude internal motion. Previous calculations made by, for example, Carney and Porter [13] and Tennyson and Sutcliffe [6] have used very large numbers of basis functions to ensure adequate convergence. One reason for the large basis sets in these calculations is the use of C_{2v} rather than the full D_{3h} symmetry of H_3^+. In hyperspherical coordinates the full permutation–inversion symmetry may be relatively easily introduced and used to reduce the size of the calculation. In addition to increasing efficiency, the use of the full D_{3h} symmetry in our calculations gives unambiguous

rovibrational state assignment, which is often uncertain in highly excited states represented by basis sets of only C_{2v} symmetry.

Our results demonstrate, for H_3^+, the accuracy and efficiency of an adiabatic representation in hyperspherical coordinates. The present results for the SDL surface are in very good agreement with the variational calculations of Tennyson and Sutcliffe, although the present calculation uses appreciably smaller basis sets. Comparison of the present results with the results of Carney and Porter for the CP surface show significant deviations for vibrational-overtone energies. The discrepancy increases with vibrational energy, indicating that these states were not fully converged in the calculations of Carney and Porter and demonstrating the difficulty in representing the high vibrational states of H_3^+ in terms of normal-mode harmonic basis functions.

In the present perturbative treatment of non-adiabatic radial–angular coupling the zeroth-order energy E_0 is rigorously a lower bound to the exact ground-state energy. Comparison with the full Brillouin–Wigner result, in which all non-adiabatic coupling terms are retained, shows the accuracy of an adiabatic separation of radial and angular motion for the ground state of H_3^+. Inclusion of the non-adiabatic correction terms into the ground-state energy causes an energy shift of only about 0·1%. However, in highly excited states this adiabatic separation is found to be less appropriate. Attempts to converge states even halfway to dissociation failed. In this region the non-adiabatic matrix elements are significant, which, together with an increased density of rovibrational levels, leads to an instability in the iterative Brillouin–Wigner perturbation series. The non-adiabatic matrix elements peak at around $\rho = 1{\cdot}8$ Å, where the angular-potential minima shifts most rapidly from an equilateral geometry found at small ρ to the atom–diatom dissociation limit appropriate at large ρ. The present calculations show that the non-adiabatic matrix elements are small at large values of ρ. An adiabatic separation may therefore be appropriate for rovibrational states in the vicinity of the dissociation limit where the large-ρ portion of the potential is essentially probed. Rovibrational calculations in this region, which might explain the fascinating experiments of Carrington and co-workers [38], would be extremely difficult in the present set of hyperspherical coordinates. A more suitable choice would be the symmetric hyperspherical coordinates introduced by Pack [23], in which the BF z axis lies in the molecular plane.

Finally, in the Smith and Whitten hyperspherical coordinate system the body-fixed axes adjust smoothly as the molecule vibrates, with the z axis perpendicular to the molecular plane. This choice is optimum for an angular-momentum decoupling approximation in oblate-top molecules. Tests of this approximation for the low rotational states of H_3^+ demonstrate good agreement (to within $2\,cm^{-1}$) with exact rovibrational calculations. This suggests that the calculation of high rotational states may be feasible in hyperspherical coordinates if an angular-momentum decoupling approximation is used to reduce the size of the calculation.

References

[1] ECKART, C., 1935, *Phys. Rev.*, **45**, 552.
[2] SUTCLIFFE, B. T., 1983, *Molec. Phys.*, **48**, 561.
[3] BARTHOLOMAE, R., MARTIN, D., and SUTCLIFFE, B. T., 1981, *J. molec. Spectrosc.*, **87**, 367.
[4] TENNYSON, J., and SUTCLIFFE, B. T., 1982, *J. chem. Phys.*, **77**, 4061.
[5] TENNYSON, J., and SUTCLIFFE, B. T., 1983, *J. chem. Phys.*, **79**, 43.
[6] TENNYSON, J., and SUTCLIFFE, B. T., 1984, *Molec. Phys.*, **51**, 887.

[7] TENNYSON, J., and SUTCLIFFE, B. T., 1986, *Molec. Phys.*, **58**, 1067.
[8] SMITH, F. T., 1962, *J. math. Phys.*, **3**, 735; Whitten, R. C., and Smith, F. T., 1968, *J. math. Phys.*, **9**, 1103.
[9] JOHNSON, B. R., 1980, *J. chem. Phys.*, **73**, 5051.
[10] FREY, J. G., and HOWARD, B. J., 1985, *Chem. Phys.*, **99**, 415.
[11] PACK, R. T., 1974, *J. chem. Phys.*, **60**, 633.
[12] SCHINKE, R., DUPUIS, M., and LESTER, W. A., 1980, *J. chem. Phys.*, **72**, 3909.
[13] CARNEY, G. D., and PORTER, R. N., 1976, *J. chem. Phys.*, **65**, 3547.
[14] DYKSTRA, C. E., and SWOPE, W. C., 1979, *J. chem. Phys.*, **70**, 1.
[15] MEYER, W., BOTSCHWINA, P., and BURTON, P., 1986, *J. chem. Phys.*, **84**, 891.
[16] CARNEY, G. D., 1980, *Molec. Phys.*, **39**, 923.
[17] CARNEY, G. D., and PORTER, R. N., 1980, *Phys. Rev. Lett.*, **45**, 537.
[18] CARNEY, G. D., ADLER-GOLDEN, S. M., and LESSESKI, D., 1986, *J. chem. Phys.*, **84**, 3921.
[19] HAMILTON, I., 1987, *J. chem. Phys.*, **87**, 774.
[20] MILLER, S., and TENNYSON, J., 1988, *J. molec. Spectrosc.*, **128**, 530.
[21] FREY, J. G., and HOWARD, B. J., 1985, *Chem. Phys.*, **99**, 427.
[22] WHITNALL, R. M., and LIGHT, J. C., 1989, *J. chem. Phys.*, **90**, 1774.
[23] PACK, R. T., and PARKER, G. A., 1987, *J. chem. Phys.*, **87**, 3888.
[24] HIRSHFELDER, J. O., and DAHLER, J. S., 1956, *Proc. Natl Acad. Sci. U.S.A.*, **42**, 363.
[25] BARTLETT, P., 1985, D.Phil. thesis, Oxford University.
[26] ECKART, C., 1934, *Phys. Rev.*, **46**, 383.
[27] VAN VLECK, J. H., 1935, *Phys. Rev.*, **47**, 487.
[28] BRINK, D. M., and SATCHLER, G. R., 1979, *Angular Momentum* (Oxford University Press).
[29] ABRAMOWITZ, M., and STEGUN, I. A., 1965, *Handbook of Mathematical Functions* (Dover).
[30] CHISHOLM, M. S., 1976, *Group Theoretical Techniques in Quantum Chemistry* (Academic Press).
[31] CASHION, J. K., 1963, *J. chem. Phys.*, **39**, 1872.
[32] EPSTEIN, S. T., 1966, *J. chem. Phys.*, **44**, 836.
[33] CHILD, M. S., 1974, *Molecular Collision Theory* (Academic Press).
[34] BONDI, D. K., CONNOR, J. N. L., MANZ, J., and ROMELT, J., 1983, *Molec. Phys.*, **50**, 467; ROMELT, J., 1983, *Int. J. quantum Chem.*, **24**, 627.
[35] WATSON, J. K. G., 1984, *J. molec. Spectrosc.*, **103**, 350.
[36] WATSON, J. K. G., FOSTER, S. C., MCKELLAR, A. R. W., BERNATH, P., AMANO, T., PAN, F. S., CROFTON, M. W., ALTMAN, R. S., and OKA, T., 1984, *Can. J. Phys.*, **62**, 1875.
[37] TENNYSON, J., and SUTCLIFFE, B. T., 1986, *J. chem. Soc. Faraday Trans. 2*, **82**, 1151.
[38] CARRINGTON, A., and KENNEDY, R. A., 1984, *J. chem. Phys.*, **81**, 91.